NASA TECHNICAL MEMORANDUM 107662

FINITE-ELEMENT ANALYSES AND FRACTURE SIMULATION IN THIN-SHEET ALUMINUM ALLOY

J. C. Newman, Jr., D. S. Dawicke, and
C. A. Bigelow

AUGUST 1992

Also published in the Proceedings of the International Workshop on Structural Integrity of Aging Airplanes, Atlanta, Georgia, March 31-April 2, 1992.

National Aeronautics and
Space Administration
Langley Research Center
Hampton, Virginia 23665-5225

FINITE-ELEMENT ANALYSES AND FRACTURE SIMULATION IN THIN-SHEET ALUMINUM ALLOY

J. C. Newman, Jr.
NASA Langley Research Center
Hampton, Virginia

C. A. Bigelow
NASA Langley Research Center
Hampton, Virginia

D. S. Dawicke
Analytical Services and Materials, Inc.
Hampton, Virginia

ABSTRACT

A two-dimensional, elastic-plastic finite-element analysis was used with a critical crack-tip-opening angle (CTOA) fracture criterion to model stable crack growth in thin-sheet 2024-T3 aluminum alloy under monotonic loading after precracking at different cyclic stress levels. Tests were conducted on three types of specimens: middle-crack, three-hole-crack and blunt-notch tensile specimens. An experimental technique was developed to measure CTOA during crack growth initiation and stable tearing using a high-resolution video camera and recorder. Crack front shapes were also measured during initiation and stable tearing using a fatigue marker-load technique. Three-dimensional elastic-plastic finite-element analyses of these crack shapes for stationary cracks were conducted to study the crack-front opening displacements.

Predicted load against crack extension on middle-crack tension specimens agreed well with test results even for large-scale plastic deformations. The analyses were able to predict the effects of specimen size and precracking stress history on stable tearing. Predicted load against load-line displacements agreed well with test results up to maximum load but the analyses tended to overpredict displacements as cracks grew beyond the maximum load under displacement-controlled conditions. During the initiation phase, the measured CTOA values were high but decreased and remained nearly constant after a small amount of stable tearing. The constant value of CTOA agreed well with the calculated value from the finite-element analysis. The larger CTOA values measured at the sheet surface during the initiation phase may be associated with the crack tunneling observed in the tests. Three-dimensional analyses for nonstraight crack fronts predicted much higher displacements near the free surface than in the interior.

INTRODUCTION

The aging aircraft research being conducted worldwide is aimed at developing and implementing advanced fatigue and fracture mechanics concepts into the damage tolerance analysis meth-

odology for the current and next generation fleets. The phenomenon of "flapping" provided the early motivation for much of this research. Flapping is the process by which a small region of a cracked fuselage structure peels open, leading to safe decompression. Whereas a single crack in a fuselage structure produces flapping, tests on simulated fuselages with multi-site or multi-element damage (MSD or MED) are showing fuselage failures without safe decompression [1]. One of the objectives in the NASA Aging Aircraft Research Program [2] is to develop the methodology to predict flapping or failure in damaged fuselage structures using a finite-element shell code with global-local adaptive mesh capabilities and appropriate local fracture criteria to predict progressive failure in complex structures. The present research focuses on the development of the local failure criteria using the finite-element method.

Stable crack growth in metallic materials under mode I (tensile) loading has been studied extensively using elastic-plastic finite-element methods [3-10]. These studies were conducted to develop efficient techniques to simulate crack extension and to examine various local and global fracture criteria. Proposed fracture criteria include crack-tip stress or strain, crack-tip-opening displacement or angle, crack-tip force, energy release rates, J-integral, and the tearing modulus. Of these, the crack-tip-opening angle (CTOA) or displacement (CTOD) at a specified distance from the crack tip was shown to be the most suited for modeling stable crack growth and instability during the fracture process [5,9,10]. Newman [11] used critical CTOD values obtained from compact specimens to predict failure loads within about 10 percent of experimental failure loads for several crack configurations in two aluminum alloys and a very ductile steel. Brocks and Yuan [12], Newman et al. [13] and Demofonti and Rizzi [14] found that, for various materials and thicknesses, CTOD or CTOA was nearly constant after a small amount of crack growth. In some cases, the region of stable tearing where CTOA or CTOD was not constant appears to be related to thickness but this region has not been defined quantitatively and needs to be studied further.

Numerous investigators [15-20] have also experimentally measured CTOD or CTOA during the fracture process. Luxmoore et al. [15] showed that CTOA was constant from the onset of stable crack growth in two aluminum alloys, but found different values for different crack configurations (middle-crack and double-edge crack tension specimens). Paleebut [16] measured CTOD at the initiation of stable tearing in compact specimens made of two aluminum alloys; these results agreed well with numerical values [11] used to model initiation, stable tearing and instability. Experiments conducted by Schwalbe and Hellmann [17] correlated a modified CTOD parameter with crack extension data for various specimen types. Reuter et al. [18], using microtopography [19], measured CTOD at the initial crack front location and

found a nearly linear relation with crack extension for low-strength steel. These results imply that CTOA was nearly constant from initiation. Recently, Kobayashi et al. [20], using a fracture surface topography analysis (FRASTA), measured CTOA on thin-sheet aluminum alloy and found that CTOA was nearly constant after the blunting process.

The objective of the present paper is to use the critical CTOA fracture criterion to study crack initiation and stable tearing in thin-sheet 2024-T3 aluminum alloy material used in aircraft fuselage construction. The fracture sequence in thin-sheet aluminum alloy is illustrated schematically in Figure 1. At low fatigue stress conditions, the crack front tunnels slightly in the interior but the fatigue surface remains relatively flat (indicated by the unshaded area). Then, during monotonic loading to failure, the crack front will tear stably under nearly flat fracture conditions and begin to develop shear lips (at 45^0) through the thickness (indicated by the shaded area in Fig. 1). At the end of the transition region, the fracture surface is completely a shear mode fracture, tearing on a 45^0 plane. Under high fatigue stresses, the crack surface may have already completed the transition to the shear mode during the fatigue cycling; thus, during monotonic loading, the stable crack growth is completely shear mode fracture.

A two-dimensional (2D), elastic-plastic finite-element analysis (FEA) was used to model the fracture process after growing a crack under a precracking stress history. Comparisons are made between measured and calculated applied stress against crack extension and applied stress against load line displacements for small and large width middle-crack tension M(T) specimens. A videographic technique was developed to measure the CTOA during initiation and stable tearing. The measurements were compared with the critical CTOA values (ψ_c) determined from the 2D finite-element analyses. The effects of precracking stress history on the fracture process were also studied. Crack-front shapes were measured during initiation and stable tearing using a fatigue marker-load technique. Three-dimensional, elastic-plastic finite-element analyses of these crack shapes for stationary cracks were conducted to assess the impact of non-straight crack fronts on crack-opening displacements.

MATERIAL, SPECIMENS AND EXPERIMENTAL PROCEDURES

Tests were conducted on the three specimen types shown in Figure 2, middle-crack, blunt notch and three-hole-crack tension specimens. All specimens were made of 2024-T3 aluminum alloy sheet material ranging in thicknesses from 0.05 to 0.09 inches. The 0.09 inch thick material was obtained from a special NASA Langley stock (purchased in the 1950's) whereas the 0.05 and 0.07 inch thick materials are of a more recent vintage.

Fracture tests were conducted on middle-crack tension M(T) specimens (Fig. 2(a)) in all thicknesses. Two specimen half-widths were tested (w = 1.5 and 5.9 inches). The M(T) specimens were fatigue precracked at either a low or high stress level (at R = 0) to produce an initial crack. The initial crack-length-to-width (c_i/w) ratio was nominally 1/3 for all M(T) specimens. The specimens were loaded under displacement control and crack extension (Δc) was measured using a 60X microscope during periodic hold times. Crack-opening displacements were measured at the centerline of the crack. On some M(T) specimens, the crack-front shapes were also measured during initiation and stable tearing using a fatigue marker-load technique. These tests were stopped after various amounts of crack extension and fatigue (high R-ratio) marker loadings were applied. The fatigue precracking and marker loading regions resulted in lighter regions on the fracture surface, distinguishable from the darker regions which resulted from the stable tearing. The interface between the light and dark regions represented the crack front shape after precracking and after stable tearing.

The blunt-notch specimen, Figure 2(b), was used to verify whether the 2D FEA could model large-scale plasticity deformations. These test specimens were similar to the M(T) specimens except that a small hole (diameter of 0.05w) was drilled at both ends of a saw-cut (c/w = 1/3). The holes were polished to help prevent premature fracture. Displacements were measured at the centerline and at both notch roots using ring gages. The specimens were loaded under displacement control until the specimen fractured.

A specially designed three-hole-crack tension specimen [21] (Fig. 2(c)) was used to measure CTOA in a structurally-configured specimen. The three-hole-crack specimen has a stress-intensity factor solution like that of a cracked, stiffened panel [22]. The specimen dimensions and stress-intensity factor solution are given in Reference 21. The specimen width, w, was 10 inches and the initial fatigue crack length, c_i, was 0.5 inches. The specimen was loaded under displacement control and crack extension (Δc) was, again, measured with the 60X microscope during periodic hold times.

A photographic technique was developed to measure CTOA during crack initiation and stable tearing. A high-resolution video camera (500X) connected to a video recorder was used to record the fracture process for several middle-crack tension specimens. During crack extension, the camera was adjusted to focus ahead of the crack tip so that when the crack grew, it would grow into the view of the camera. A typical video frame is shown in Figure 3. In each frame, the critical value of CTOA (ψ_c) was measured at several distances behind the crack tip.

This was done to determine what effect, if any, that varying this distance would have on the CTOA measurement.

FINITE-ELEMENT ANALYSES

Two elastic-plastic finite-element codes, ZIP2D [23] and ZIP3D [24], were used in the current study. The elastic-plastic analysis of both codes employs the initial-stress concept [25] which is based on incremental flow theory and small strain assumption. A multi-linear representation of the uniaxial stress-strain curve for 2024-T3 was used in the analyses with the von Mises yield criterion. The three specimen configurations shown in Figure 2, middle-crack tension, blunt notch and three-hole-crack tension, were analyzed.

ZIP2D, a two-dimensional analysis, was used to study stable crack growth in the M(T) specimens and large-scale plastic deformations in the blunt-notch specimen under plane-stress and plane-strain conditions. ZIP2D uses two-dimensional, constant-strain, triangular elements. The mesh pattern used for the 5.9-inch-wide M(T) specimen is shown in Figure 4(a). A similar mesh pattern was used for the 1.5-inch-wide specimen. The minimum element size (d) along the line of crack extension was the same for all 2D meshes, d = 0.01875 inches. Fictitious springs were used to change boundary conditions associated with crack extension. For free nodes along the crack line, the spring stiffnesses were set equal to zero; for fixed nodes, the stiffnesses were assigned extremely large values. See Reference 23 for details of the elastic-plastic finite element analysis with crack extension. To model fatigue precracking, the initial crack length was set equal to the initial saw-cut length. Cyclic loads were applied to the model and the crack was extended one element length each time the maximum fatigue stress (S_{max}) was reached. Once the crack had grown to the desired crack length, monotonic loading (displacement control) was applied and the crack growth was governed by a critical CTOA criterion.

A critical CTOA (ψ_c) criterion is equivalent to a critical CTOD (δ_c) value at a specified distance d behind the crack tip since $\psi_c = 2 \tan^{-1} (\delta_c/2d)$. Whenever the CTOD equaled or exceeded a preset critical value (δ_c) during incremental loading, the crack tip node was released and the crack advanced to the next node. This process was repeated until crack growth became unstable under load control or the crack reached the desired length under displacement control. As will be explained later, the critical ψ_c value was analytically determined to match the average maximum load measured in several tests of M(T) specimens.

The elastic-plastic analyses of M(T) specimens with stationary straight or curved crack fronts were done using ZIP3D [24]. ZIP3D uses eight-noded, hexahedral elements. Six layers of elements were used through the half-thickness (z-direction), as shown in the Figure 4(b). The thicknesses of each layer were 0.005615, 0.005635, 0.01125, 0.01125, 0.00765, and 0.0036 inches, respectively, where the thinnest layer was on the specimen surface. In the 3D analysis, the crack length was held constant ($2c/w = 0.5$) and no crack growth was considered. The minimum element size d at the crack front was 0.004 inches ($d/c = 0.0016$). As will be described later, the crack-front shapes for the non-straight cracks were determined from experimental observations. To model the nonstraight crack fronts, the mesh shown in Figure 4(b) was modified. The z-coordinates of a portion of the mesh surrounding the crack tip ($0.7c < x < 1.3c$ and $0.0 < y < 0.3c$) were changed to correspond to the measured crack fronts.

RESULTS AND DISCUSSIONS

Blunt-Notch Tests and Analyses

Because the FEA codes employ the small-strain assumption, their ability to model large-scale plastic deformations was a concern. The blunt-notch specimen, Figure 2(b), was used to examine this issue. In this specimen, the notch length remains fixed while the specimen undergoes intense plastic deformations. Displacements were measured at the center of the notch and at both notch roots during monotonic loading to failure. Figure 5 shows a comparison of applied stress against notch-root displacement from the test (symbols) and from 2D FEA (solid curve). The V_2-displacements were measured and calculated at the locations shown in the insert. The solid symbol is the last reading before the specimen failed. The analysis agreed quite well with the test results especially after net-section yielding (the plateau). In the early stages of deformation, the analysis was about 10 percent lower than the measured displacements indicating that the finite-element model was probably too stiff. Similar agreement between measured and predicted centerline displacements was found for both the 2D analysis with a sharp notch and the 3D analysis with a non-growing crack. These results confirm that both the 2D and 3D analyses are able to model the large-scale plastic deformations that are present during the fracture of thin-sheet aluminum alloys.

Stable Tearing Tests and Analyses

The results of three M(T) fracture tests using three material thicknesses are shown in Figure 6 where the applied stress (S) is plotted against crack extension. All of these specimens were fatigue precracked at a low stress level, then loaded monotonically until failure. These test re-

sults were used to determine the critical CTOA (ψ_c). A value of ψ_c was selected so that the FEA would produce a maximum load equal to the average of the maximum loads of these tests. The critical angle ψ_c was 6.1^o under plane-stress conditions. Calculations from the FEA using ψ_c are shown by the solid curve in Figure 6. The agreement between the calculations and the test data near and beyond maximum load is reasonable considering that the net-section stresses S_n are between the yield stress and the ultimate tensile strength. Calculations under plane-strain conditions using the same critical angle are shown by the dashed curve. Surprisingly, these results agreed well over the complete range of data. However, this agreement is fortuitous because the thin-sheet material is definitely not in a condition of plane strain.

Tests were conducted on specimens that were fatigue precracked at both high and low stress levels. The analyses and test data are compared in Figure 7 for the 0.07-inch thick material. The solid symbols show the measured crack extension results after the high precracking history (S_{max} = 22.5 ksi). These results show that the higher fatigue stress delayed the crack initiation point to an applied stress level slightly higher than the maximum fatigue stress. The 2D FEA results for the high precrack stress, shown by the solid curve, agreed very well with the test data. In the analysis, the high fatigue stress caused fatigue crack closure to develop while the crack grew under fatigue. The crack tip was shielded by a wake of material that had been plastically deformed and, thus, a higher applied stress level was required to reach the critical angle ψ_c. The open symbols and the dashed line show the results for the low precrack stress. The test results and the analysis also agreed well for low fatigue stress levels. As previously discussed, a crack grown under a low fatigue stress will have to go through a transition to the shear mode fracture in the early stages of crack growth. Additionally, as will be discussed later, in the early stages of growth, the crack growth lags on the surface and grows more in the interior. Thus, the measured crack extensions on the surface may not be indicative of the average crack extension. The high fatigue stress test did not have to transition to shear mode fracture and, as will be shown later, crack growth through the thickness is nearly uniform during shear mode fracture.

Figure 8 shows a comparison of measured and predicted crack extensions for a smaller width M(T) specimen using $\psi_c = 6.1^o$. These results are quite similar to those shown for the wide specimens, that is the analysis (curve) overpredicted crack extension before maximum load. Again, crack tunneling may be the reason for the disagreement. However, the analysis predicted a maximum applied stress within 4 percent of the experimental results. These results

indicate that the critical CTOA is able to predict the effects of specimen size on maximum failure loads.

A comparison of measured and predicted load-line displacements (displacements remote from the crack) for the wide M(T) specimens is shown in Figure 9. The symbols show the measurements made on the three specimen thicknesses. Here the thinnest specimen (B = 0.05 inches) tended to show higher displacements beyond maximum applied stress but this may have been due to the thinner specimen reaching a higher maximum applied stress level than the other specimens. Again, two analyses were made using the critical CTOA ψ_c of 6.1^o. One analysis was made under plane-stress conditions (solid curve); the other was made under plane-strain conditions (dashed curve). As expected, the plane-strain analysis was too stiff. However, beyond the maximum applied load, the plane-stress analysis predicted more displacement than was observed in the tests. The reason for this discrepancy is still under investigation. It may be related to constraint effects because the test data fell between the plane-stress and plane-strain results but closer to the plane-stress results.

Comparison of Measured and Calculated CTOA

As shown previously in Figure 2, the CTOA was measured during the fracture process on several M(T) specimens and one three-hole-crack specimen. The results for one of the M(T) specimens is shown in Figure 10. The critical angle ψ_c is plotted against crack extension, Δc. For each increment of crack extension, one to three values of ψ_c were measured at varying distances behind the crack tip. The vertical lines indicate the location of the initial crack tip c_i, the transition to shear mode fracture and the peak load. The measured ψ_c before the transition are between 7.5 and 15^o but after transition they appear to have an average value of about 6.5^o. The solid horizontal line is the ψ_c value (6.1^o) determined from the 2D FEA. The dashed horizontal line is the measured angle from the FRASTA method [20] on a thinner 2024-T3 aluminum alloy sheet. In the transition region, the agreement between the present measurements and the FRASTA method is quite good. The overall results from the present measurements are not vastly different from those presented in the literature for other materials.

The measured ψ_c values from a three-hole-crack specimen are shown in Figure 11. Again, ψ_c is plotted against crack extension. The vertical lines indicate the locations of the initial crack tip c_i, the transition to shear mode fracture, the region of decreasing crack driving force (which begins at the location of the peak stress-intensity factor) and the center-line of the large holes. Each data point shown is the average of three to four ψ_c measurements made at

each value of crack extension. The trends are, again, similar to those shown in Figure 10. The critical ψ_c determined from the analysis of the M(T) specimens is shown by the solid horizontal line at 6.1^{o}. Again, higher values of ψ_c were measured at crack initiation. The experimental and analytical results are in excellent agreement after the transition region.

Crack Front Shape

To understand the high CTOA values measured during crack initiation, a series of test were conducted to measure the crack front shapes during the fracture process, especially in the early stages before the transition to the shear mode fracture. Figure 12 shows measurements for crack-front shapes from three tests for specimens with a thickness B of 0.09 inches. The symbols represent the average values from the left and right crack tip measurements. The curves shown in the figure were used to model the crack fronts in the 3D FEA. The solid circles show the tunneling that would typically result from the fatigue precracking of the specimen. The specimen was then monotonically loaded and the specimen surface in the crack-tip region was observed using a high-power microscope. When a slight amount of crack extension was observed, the loading was stopped and a fatigue marker loading was applied. The specimen was then fractured to reveal the crack shape as shown by the open circles (Stable 1). A larger amount of crack extension was measured in the interior compared to the values at the free surfaces. A second specimen was tested where a greater amount of stable crack extension was allowed before fracturing the specimen; Stable 2 shows the crack shape that was measured. Even with the extreme tunneling found in this case, the crack front still lies within the flat fracture region. The cross-hatched region shows the development of the transition from the flat fracture to the shear mode fracture region. In the third test, the Stable 3 crack front was measured during the transition to the shear mode fracture; the crack front shape is becoming nearly straight through the thickness, although now on a 45^{o} plane. These results suggest that in the early stages of stable crack growth, even in thin-sheet aluminum alloy, the fracture process is truly three dimensional.

Three-Dimensional Finite-Element Analyses

The 3D FEA code ZIP3D was used to analyze the influence of crack shape on crack-tip-opening displacement. Comparisons were made for four measured crack front shapes (Straight, Fatigue, Stable 1 and Stable 2) in the flat crack region, as shown in Figure 12. For the 3D analyses, the crack length was held constant for all crack front shapes and no crack extension was modeled. Crack-tip-opening displacements were compared at a distance d = 0.004 inches behind the crack tip; this distance corresponds to one element length (d/c = 0.0016). Normal-

ized elastic displacements for the four crack shapes are shown in Figure 13, where E is Young's modulus, S is applied stress, B is the specimen thickness (B = 0.09 inches), and V is the crack-tip-opening displacement. These results show that even modeling the small amount of tunneling found in the fatigue crack front will greatly change the crack mouth profile. All three of the curved crack fronts show a significantly larger displacement on the specimen surface (z/B = 0.5) that in the center of the specimen thickness (z/B = 0.0).

Experimentally, stable crack growth was observed at the surface at an applied stress of about 15 ksi when the crack front shape was somewhere between the Fatigue crack shape and the Stable 1 crack shape. The 3D elastic-plastic analysis was used to calculate the crack-tip-opening displacements corresponding to both the Fatigue and Stable 1 crack fronts at an applied stress of 15 ksi, as shown in Figure 14. The two curves are similar. The displacements calculated for the Fatigue crack front are 31% greater on the surface compared to the values at the center; for the Stable 1 crack front, the displacements are 44% greater on the surface compared to the center. If the 6.1^{o} determined earlier is assumed to govern the crack growth in the interior, then the surface CTOA should be 8 to 9^{o}. This agrees with the trends in ψ_c measured prior to the transition, shown earlier in Figures 10 and 11. Higher values of ψ_c were measured on the surface but lower values in the interior would control the crack growth. Crack-tip-opening displacements were also calculated for the Stable 2 crack shape at a higher applied stress level (S = 27 ksi), as shown in Figure 14. Although these crack-tip displacements show variation through the thickness, it appears that with the changing crack front shape, the displacements are becoming more uniform through the thickness.

CONCLUDING REMARKS

A two-dimensional, elastic-plastic, finite-element analysis was used with a critical crack-tip-opening angle (CTOA) fracture criterion to model stable crack growth in thin-sheet 2024-T3 aluminum alloy under monotonic loading after precracking at either low or high cyclic stress levels. Tests were conducted on three types of specimens: middle-crack, three-hole-crack and blunt-notch specimens. All specimens were subjected to remote tensile loading and tested under displacement-control conditions. The specimen thicknesses ranged from 0.05 to 0.09 inches. An experimental technique was developed to measure CTOA during crack-growth initiation and stable tearing using a high-resolution video camera and recorder. Crack-front shapes were also measured during initiation and stable tearing by using a fatigue marker-load technique. Three-dimensional elastic-plastic finite-element analyses of these crack shapes for stationary cracks were also conducted to study the crack-front opening displacements.

Predicted load against load-line and notch-tip displacements under plane-stress conditions for the blunt-notch specimen agreed well with test results for large-scale plastic deformations. Comparisons made between measured and calculated load against crack extension behavior on middle-crack tension specimens agreed well even as the net-section stresses approached the ultimate tensile strength. The analyses were able to predict the effects of specimen size and precracking stress history on stable tearing. Predicted load against load-line displacements for middle-crack specimens agreed well with test results up to maximum load but the analyses tended to overpredict displacements beyond maximum load in displacement-controlled tests. During the initiation phase, the measured CTOA values from surface observations were high but they became nearly constant after a small amount of stable tearing. The average measured value of CTOA agreed well with the calculated value from the finite-element analysis. The high CTOA values measured at the sheet surface during the initiation phase may be associated with the crack tunneling that was observed in the tests. Three-dimensional analyses for non-straight crack fronts gave much higher displacements near the free surface than in the interior. The analysis methodology presented here may be used in global-local structural analysis methods to predict stable crack growth in cracked structural components.

REFERENCES

1. Maclin, J. R.: Commercial Airplane Perspective on Multiple Site Damage, Int. Conf. Aging Aircraft and Structural Airworthiness, 1991.

2. Harris, C. E.: NASA Aircraft Structural Integrity Program, NASA TM-102637, April 1990.

3. Kobayashi, A. S., Chiu, S. T. and Beeuwkes, R.: A Numerical and Experimental Investigation on the Use of the J-Integral, *Engng. Fracture Mech.*, Vol. 5, No. 2, 1973, pp. 293-305.

4. Anderson, H.: A Finite-Element Representation of Stable Crack Growth, *J. Mech. and Phys. Solids*, Vol. 21, 1973, pp. 337-356.

5. de Koning, A. U.: A Contribution to the Analysis of Slow Stable Crack Growth, National Aerospace Laboratory Report NLR MP 75035U, 1975.

6. Light, M. F., Luxmoore, A. and Evans, W. T.: Prediction of Slow Crack Growth by a Finite Element Method, *Int. J. Fatigue*, Vol. 11, 1975, pp. 1045-1046.

7. Newman, J. C., Jr.: Finite Element Analysis of Crack Growth Under Monotonic and Cyclic Loading, *ASTM STP 637*,1977, pp. 56-80.

8. Rousselier, G.: A Numerical Approach for Stable-Crack-Growth and Fracture Criteria, Fourth Int. Conf. Fracture, Canada, Vol. 3, 1977.

9. Shih, C F., de Lorenzi, H. G. and Andrews, W. R.: Studies on Crack Initiation and Stable Crack Growth, *ASTM STP 668*, 1979, pp. 65-120.

10. Kanninen, M. F., Rybicki, E. F., Stonesifer, R. B., Broek, D., Rosenfield, A. R. and Nalin, G. T.: Elastic-Plastic Fracture Mechanics for Two-Dimensional Stable Crack Growth and Instability Problems, *ASTM STP 668*, 1979, pp. 121-150.

11. Newman, J. C., Jr.: An Elastic-Plastic Finite Element Analysis of Crack Initiation, Stable Crack Growth, and Instability, *ASTM STP 833,* 1984, pp. 93-117.

12. Brocks, W. and Yuan, H.: Numerical Studies on Stable Crack Growth, ESIS Pub. 9, 1991, pp. 19-33.

13. Newman, J. C., Jr., Shivakumar, K. N. and McCabe, D. E.: Finite Element Fracture Simulation of A533B Steel Sheet Specimens, ESIS Pub. 9, 1991, pp. 117-126.

14. Demofonti, G. and Rizzi, L.: Experimental Evaluation of CTOA in Controlling Unstable Ductile Fracture Propagation, ESIS Pub. 9, 1991, pp. 693-703.

15. Luxmoore, A., Light, M. F. and Evans, W. T.: A Comparison of Energy Release Rates, the J-Integral and Crack Tip Displacements, *Int. J. Fracture,* Vol. 13, 1977, pp. 257-259.

16. Paleebut, S.: CTOD and COD Measurements on Compact Specimens of Different Thicknesses, M.S. Thesis, Michigan State University, 1978.

17. Schwalbe, K. -H. and Hellmann, D.: Correlation of Stable Crack Growth with the J-Integral and the Crack Tip Opening Displacement, GKSS Report 84/E/37, 1984.

18. Reuter, W. G., Graham, S. M., Lloyd, W. R. and Williamson, R. L.: Ability of Using Experimental Measurements of w to Predict Crack Initiation for Structural Components, ESIS Pub. 9, 1991, pp. 175-188.

19. Kobayashi, T., Irwin, G. R. and Zhang, X. J.: Topographic Examination of Fracture Surfaces in Fibrous-Cleavage Transition Behavior, *ASTM STP 827*, 1989, pp. 234-251.

20. Kobayashi, T., Giovanola, J. H., Kirkpatrick, S. W., Simons, J. W., and Holmes, B. S.: Reconstruction of Fracture Processes in Thin Aluminum Sheet Using Fracture Surface Topography Analysis (FRASTA), SRI International, Menlo Park, California, FAA Report (in progress).

21. Newman, J. C., Jr.: An Evaluation of Fracture Analysis Methods, *ASTM STP 896,* 1985, pp. 5-96.

22. Poe, C. C.: Stress Intensity Factor for a Cracked Sheet with Riveted and Uniformly Spaced Stringers, NASA TR-358, May 1971.

23. Newman, J. C., Jr.: Finite-Element Analysis of Fatigue Crack Propagation--Including the Effects of Crack Closure, Ph.D. Thesis, VPI & State University, Blacksburg, Va., May 1974.

24. Shivakumar, K. N. and Newman, J. C., Jr.: ZIP3D - An Elastic and Elastic-Plastic Finite-Element Analysis Program for Cracked Bodies, NASA TM-102753, Nov. 1990.

25. Zienkiewicz, O. C., Valliappan, S. and King, I. P., *Int. J. Numerical Methods Engng.*, Vol. 1, 1969, pp. 75-100.

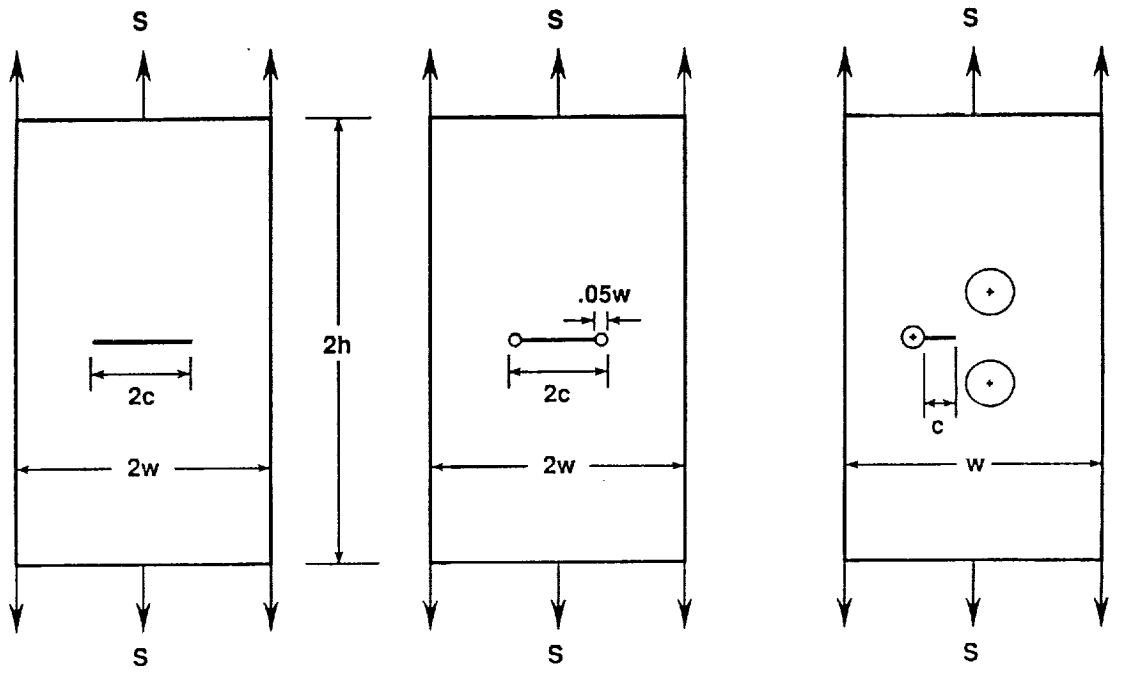

(a) Middle-crack (b) Blunt-notch (c) Three-hole-crack

Figure 1. - Specimen configurations tested and analyzed.

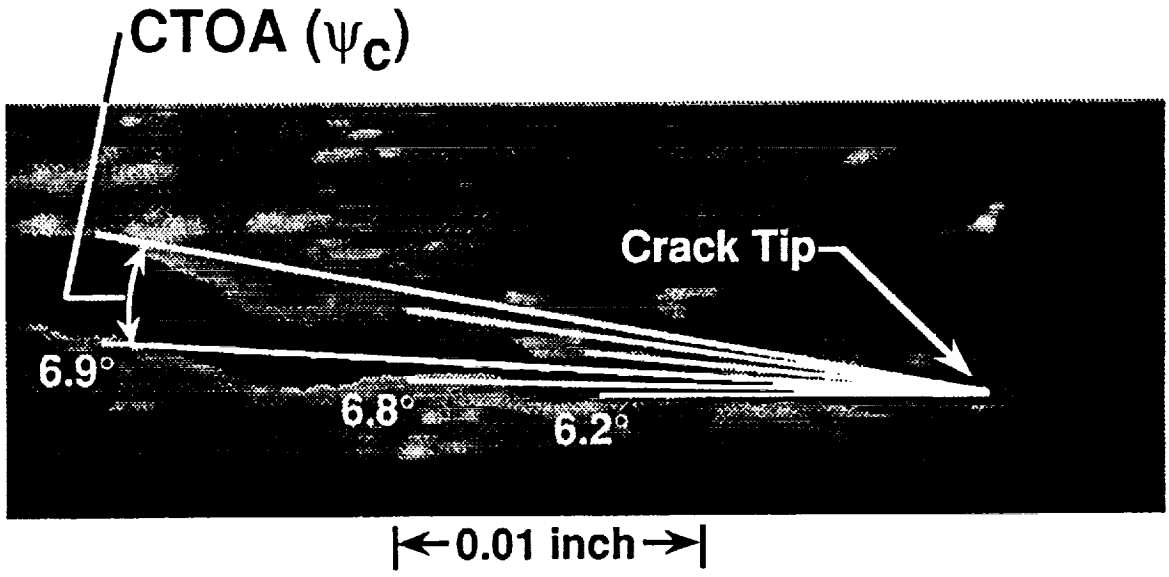

Figure 2. - Computer-enhanced high-resolution video frame of stably tearing crack.

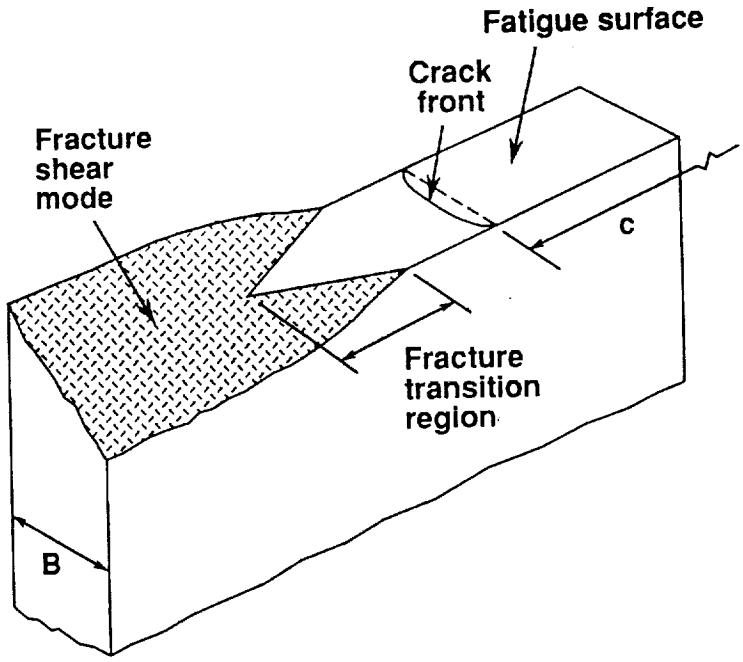

Figure 3. - Schematic of fracture surface indicating transition from a flat to a slant crack plane.

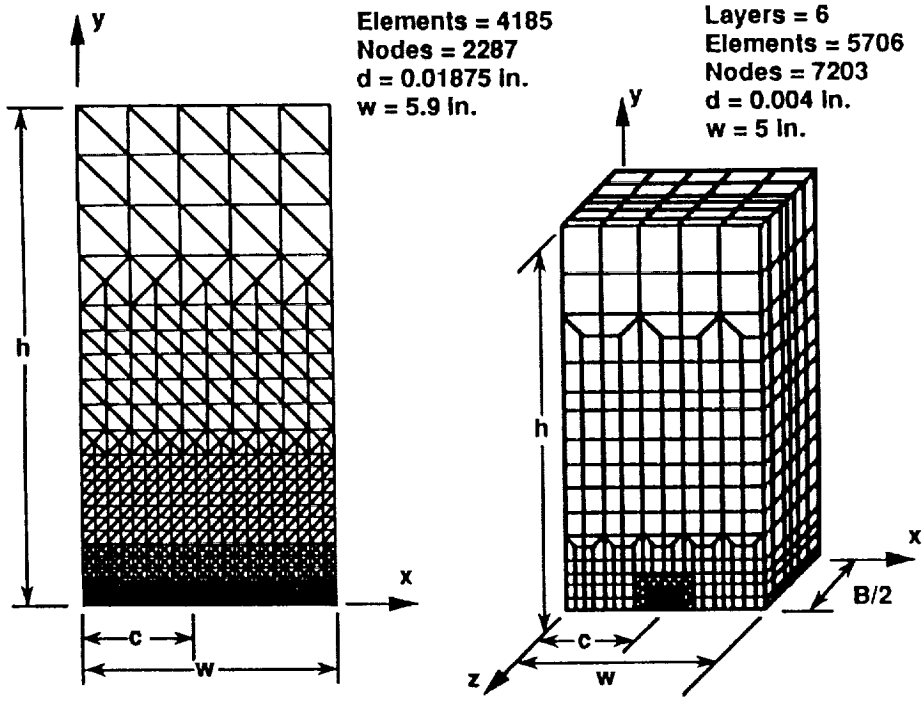

(a) Two-dimensional model (b) Three-dimensional model

Figure 4. - Typical finite-element models of middle-crack specimens.

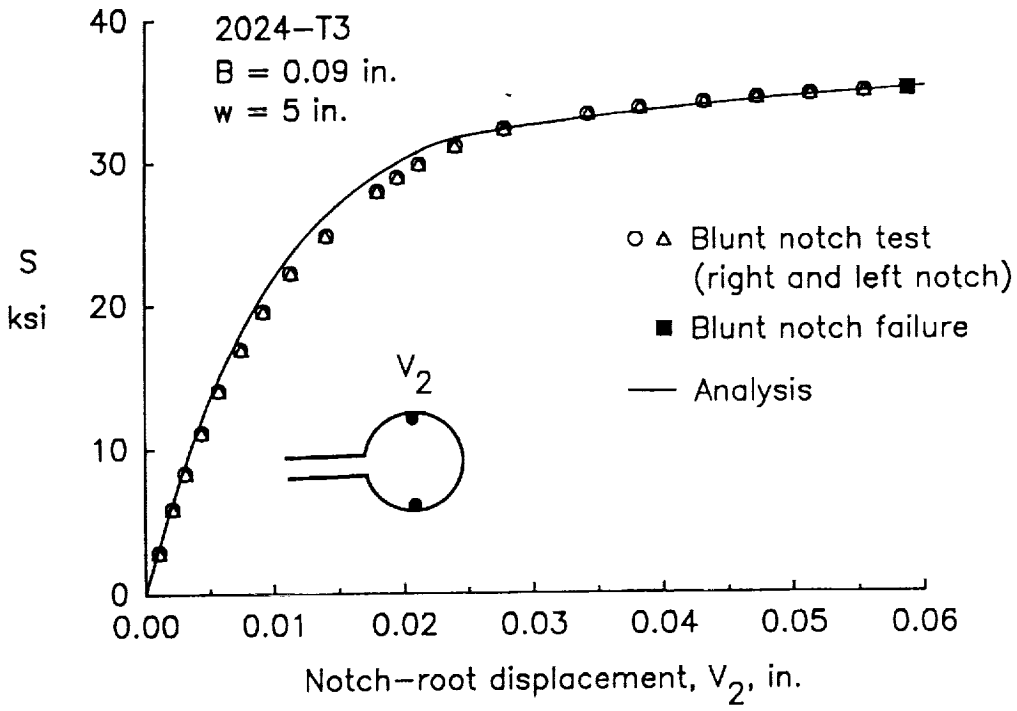

Figure 5. - Comparison of measured and predicted notch-tip displacements for blunt-notch specimen statically pulled to failure.

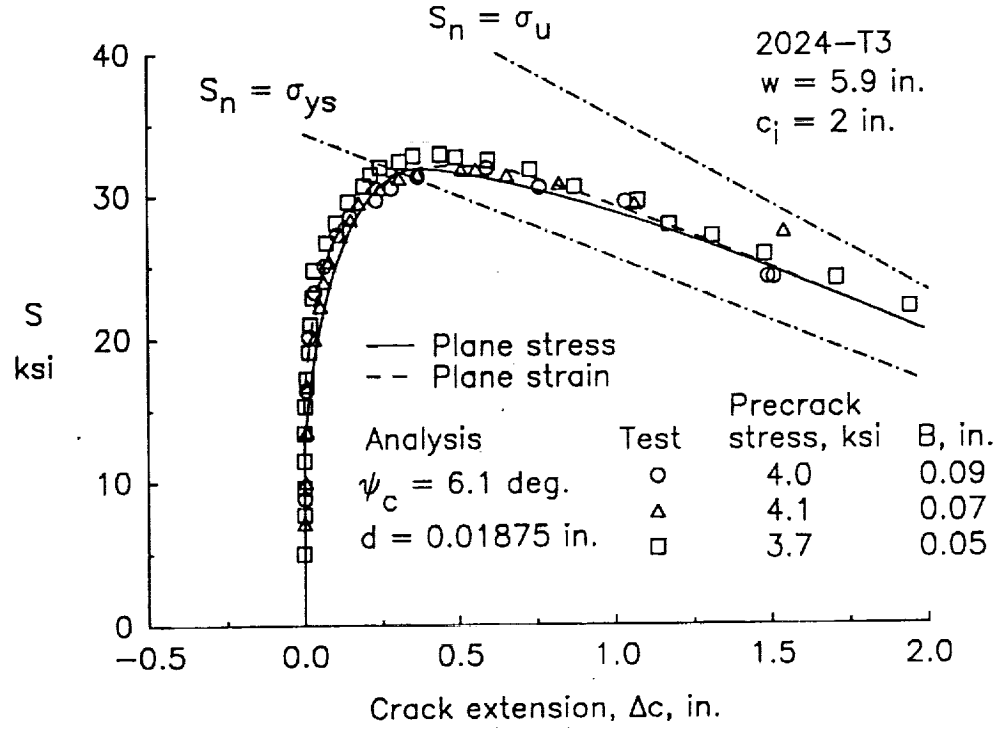

Figure 6. - Comparison of measured and predicted stable crack growth in wide M(T) specimens using critical CTOA criterion.

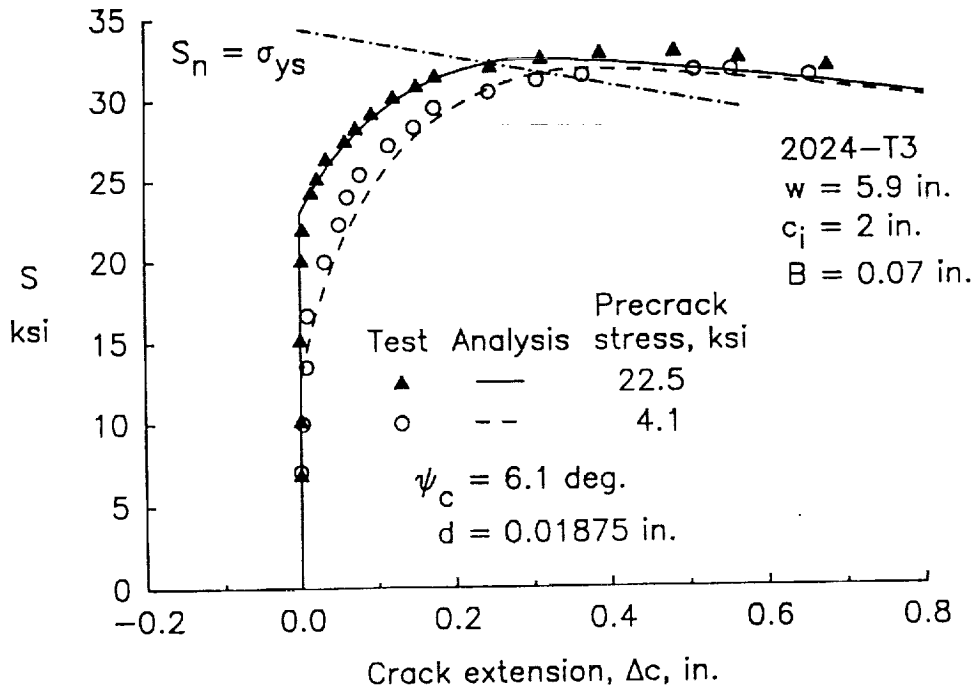

Figure 7. - Comparison of measured and predicted stable crack growth in wide M(T) specimens for low and high precracking stress.

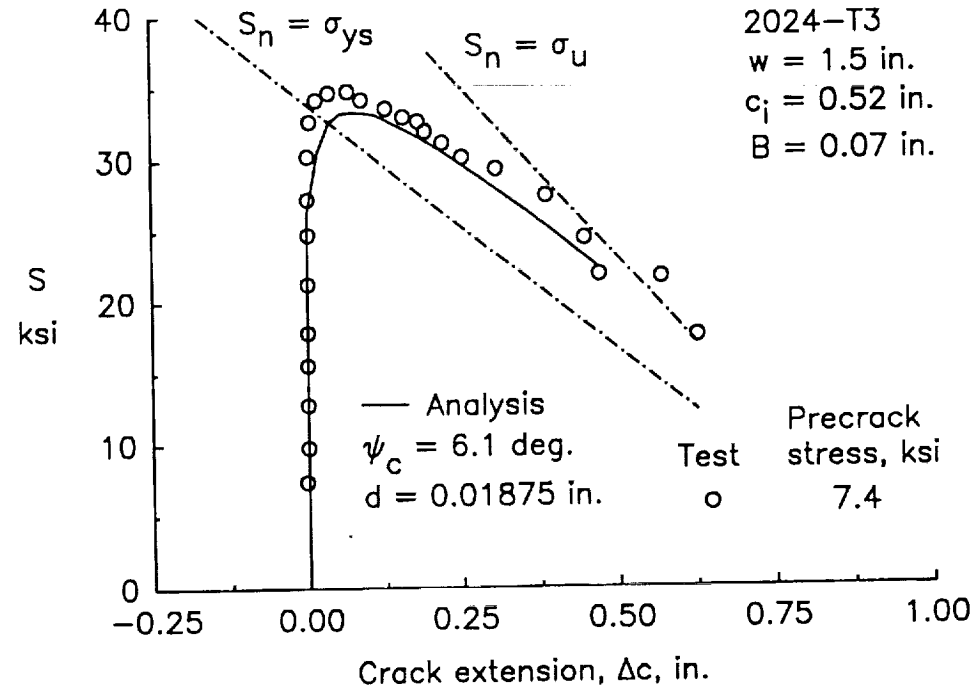

Figure 8. - Comparison of measured and predicted stable crack growth in a small width M(T) specimen using critical CTOA criterion.

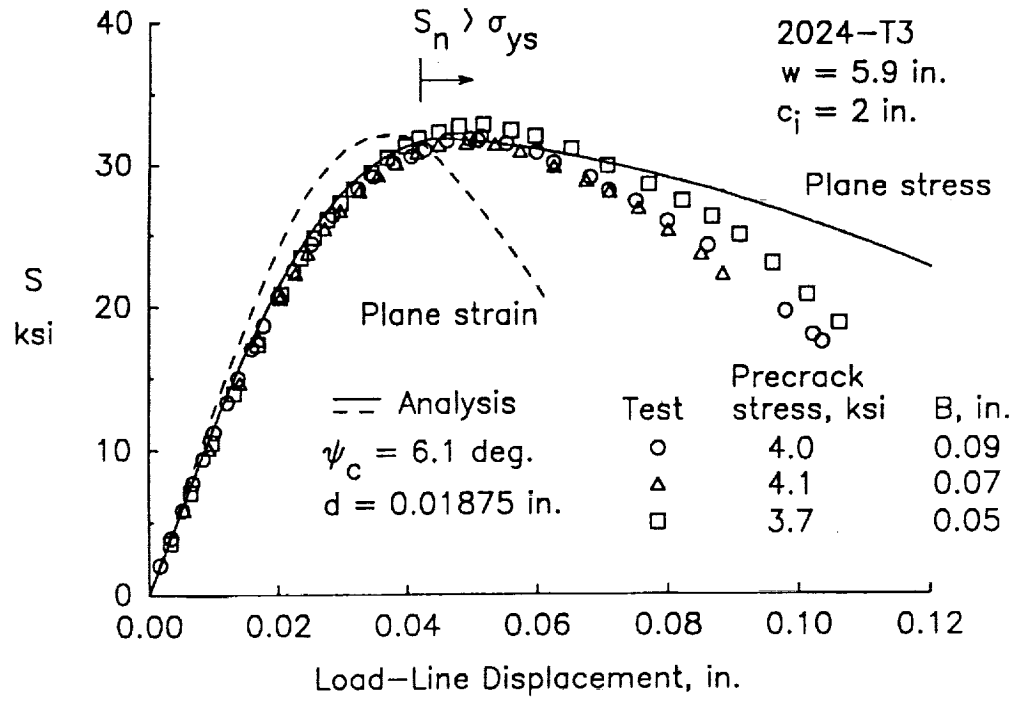

Figure 9. - Comparison of measured and predicted load-line displacements in wide M(T) specimens using critical CTOA criterion.

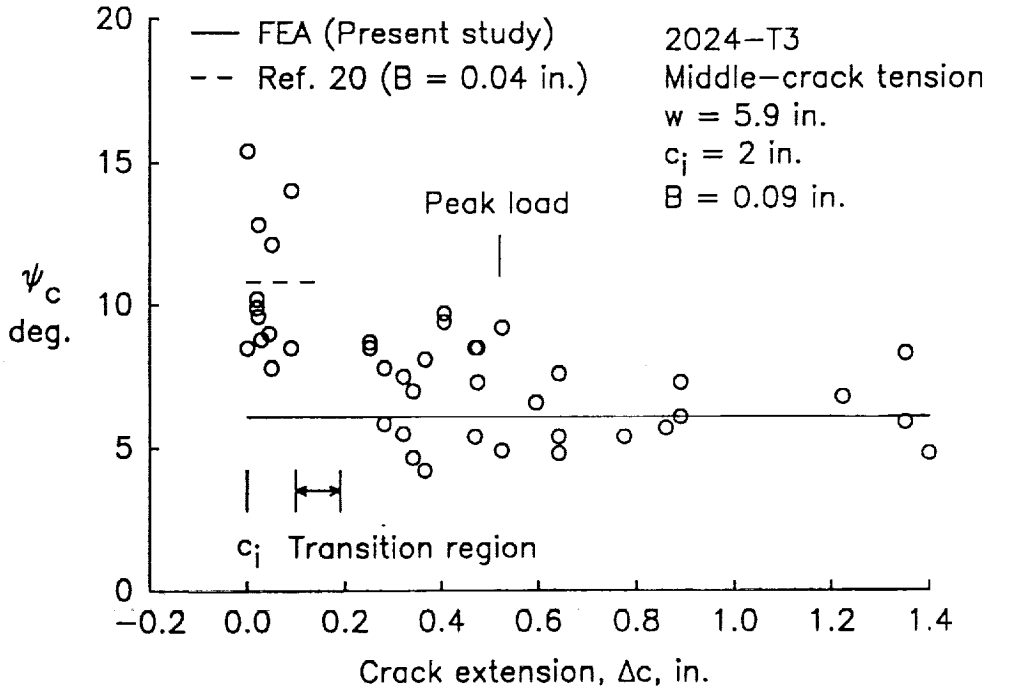

Figure 10. - Comparison of measured and calculated CTOA from M(T) specimens.

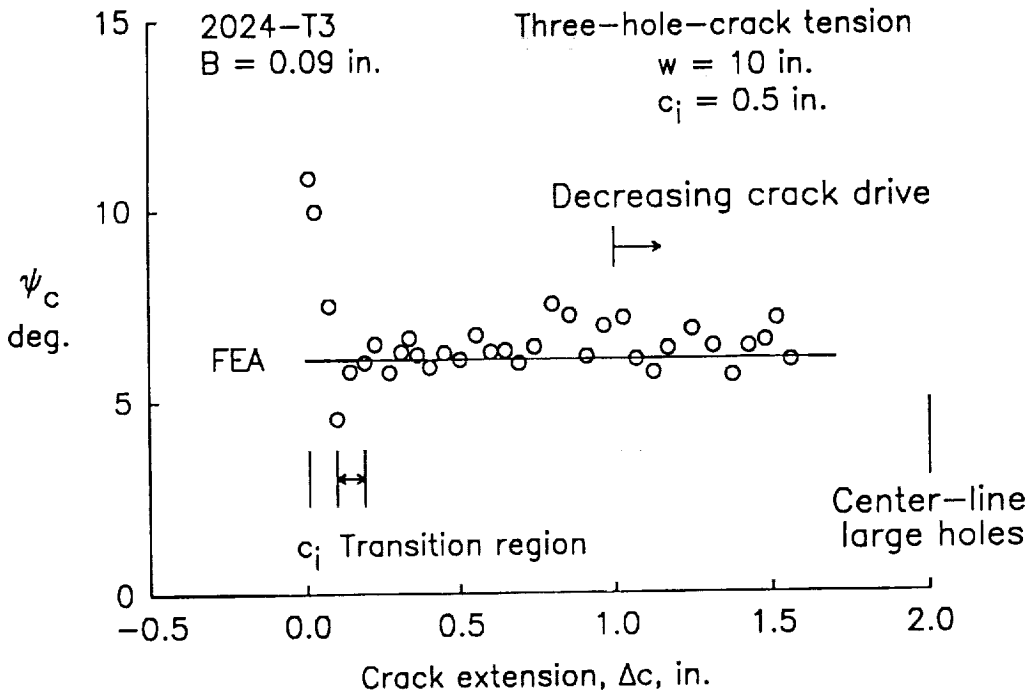

Figure 11. - Comparison of measured CTOA from a three-hole-crack specimen with calculated CTOA from M(T) specimens.

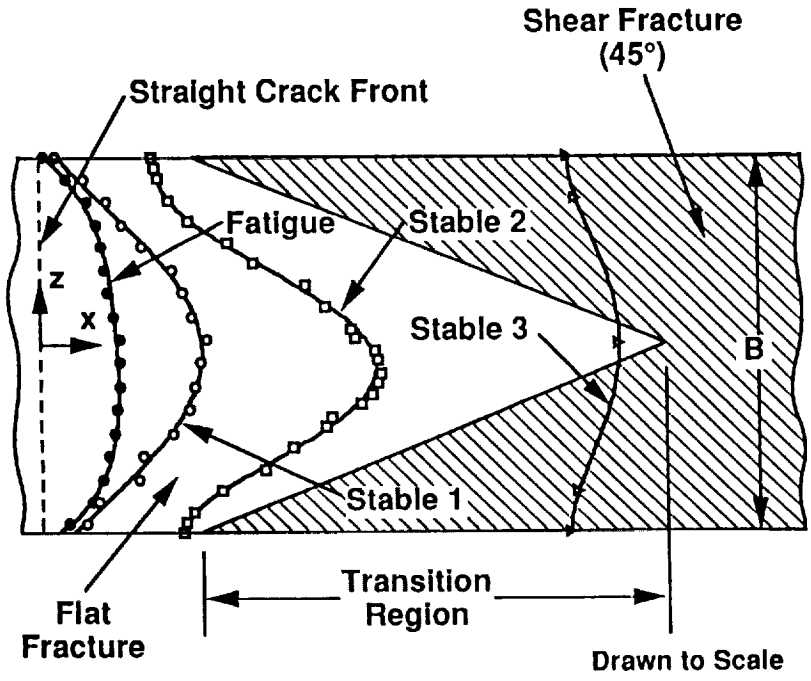

Figure 12. - Crack-front shapes measured during fatigue crack growth and stable tearing for M(T) specimens.

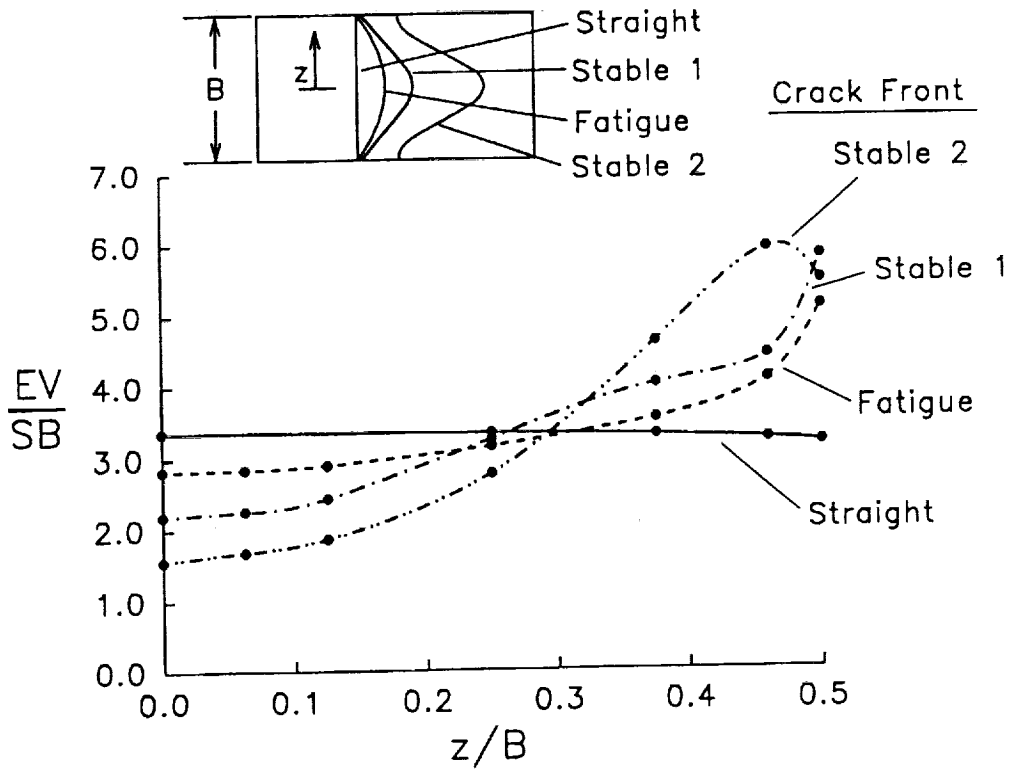

Figure 13. - Effect of crack front shape on calculated elastic crack-opening displacements for M(T) specimens using 3D FEA.

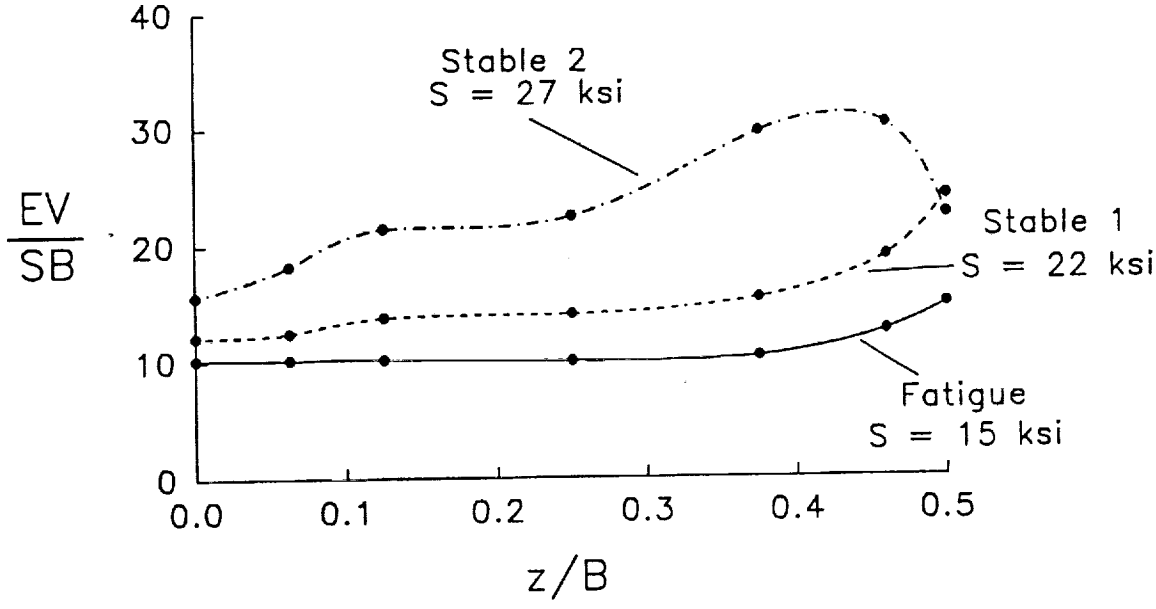

Figure 14. - Effect of applied stress on elastic-plastic crack-opening displacements for M(T) specimens using 3D FEA.

REPORT DOCUMENTATION PAGE

Form Approved
OMB No. 0704-0188

1. AGENCY USE ONLY (Leave blank)	2. REPORT DATE	3. REPORT TYPE AND DATES COVERED
	August 1992	Technical Memorandum

4. TITLE AND SUBTITLE
Finite-Element Analyses and Fracture Simulation in Thin-Sheet Aluminum Alloy

5. FUNDING NUMBERS
WU 538-02-10

6. AUTHOR(S)
J. C. Newman, Jr., D. S. Dawicke, and C. A. Bigelow

7. PERFORMING ORGANIZATION NAME(S) AND ADDRESS(ES)
NASA Langley Research Center
Hampton, VA 23665-5225

8. PERFORMING ORGANIZATION REPORT NUMBER

9. SPONSORING / MONITORING AGENCY NAME(S) AND ADDRESS(ES)
National Aeronautics and Space Administration
Washington, DC 20546-0001

10. SPONSORING / MONITORING AGENCY REPORT NUMBER
NASA TM-107662

11. SUPPLEMENTARY NOTES
Newman: Langley Research Center, Hampton, VA; Dawicke: Analytical Services & Materials, Inc., Hampton, VA; and Bigelow: Langley Research Center, Hampton, VA. Presented at the International Workshop on Structural Integrity of Aging Airplanes, Atlanta, GA; March 31-April 2, 1992.

12a. DISTRIBUTION / AVAILABILITY STATEMENT
Unclassified - Unlimited

Subject Category 39

12b. DISTRIBUTION CODE

13. ABSTRACT *(Maximum 200 words)*

A two-dimensional, elastic-plastic finite-element analysis was used with a critical crack-tip-opening angle (CTOA) fracture criterion to model stable crack growth in thin-sheet 2024-T3 aluminum alloy under monotonic loading after precracking at different cyclic stress levels. Tests were conducted on three types of specimens: middle-crack, three-hole-crack and blunt-notch tensile specimens. An experimental technique was developed to measure CTOA during crack growth initiation and stable tearing using a high-resolution video camera and recorder. Crack front shapes were also measured during initiation and stable tearing using a fatigue marker-load technique. Three-dimensional elastic-plastic finite-element analyses of these crack shapes for stationary cracks were conducted to study the crack-front opening displacements.

Predicted load against crack extension on middle-crack tension specimens agreed well with test results even for large-scale plastic deformations. The analyses were able to predict the effects of specimen size and precracking stress history on stable tearing. Predicted load against load-line displacements agreed well with test results up to maximum load but the analyses tended to overpredict displacements as cracks grew beyond the maximum load under displacement-controlled conditions. During the initiation phase, the measured CTOA values were high but decreased and remained nearly constant after a small amount of stable tearing. The constant value of CTOA agreed well with the calculated value from the finite-element analysis. The larger CTOA values measured at the sheet surface during the initiation phase may be associated with the crack tunneling observed in the tests. Three-dimensional analyses for nonstraight crack fronts predicted much higher displacements near the free surface than in the interior.

14. SUBJECT TERMS
Critical crack-tip-opening angle (CTOA); Fatigue; Fracture mechanics; Damage tolerance analysis methodology; Flapping

15. NUMBER OF PAGES
21

16. PRICE CODE
A03

17. SECURITY CLASSIFICATION OF REPORT	18. SECURITY CLASSIFICATION OF THIS PAGE	19. SECURITY CLASSIFICATION OF ABSTRACT	20. LIMITATION OF ABSTRACT
Unclassified	Unclassified		